Electronic Supplementary Information for

Origin of strong red emission in Er^{3+}-based upconversion materials: Role of intermediate states and cross relaxation

Chiho Lee[1‡], Heeyeon Park[2‡], Woong Kim[2], and Sungnam Park[1,3]**

[1]Department of Chemistry and Research Institute for Natural Sciences, Korea University, 145 Anam-ro, Seongbuk-gu, Seoul 02841, Republic of Korea

[2]Department of Materials Science and Engineering, Korea University, 145 Anam-ro, Seongbuk-gu, Seoul 02841, Republic of Korea

[3]Green School, Korea University, 145 Anam-ro, Seongbuk-gu, Seoul 02841, Republic of Korea

*Authors to whom correspondence should be addressed.

Email addresses: woongkim@korea.ac.kr & spark8@korea.ac.kr

‡ These authors contributed equally to this work

Figure S1.

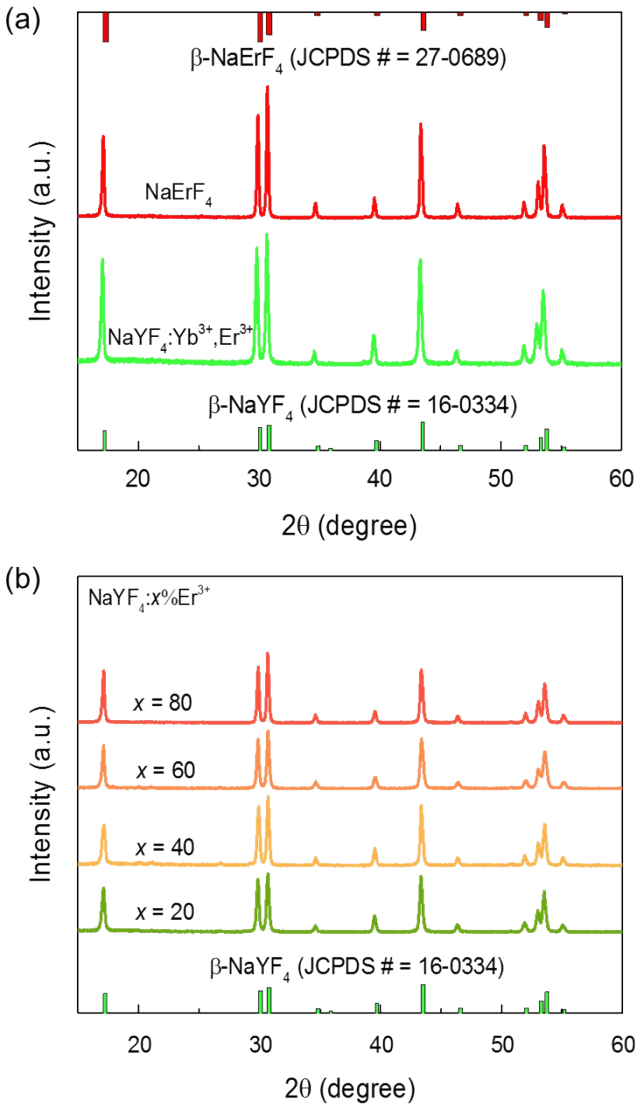

Figure S1. XRD patterns of **(a)** $NaErF_4$, $NaYF_4:Yb^{3+},Er^{3+}$ (Y^{3+}:Yb^{3+}:Er^{3+}=78:20:2), and **(b)** $NaYF_4$: x%Er^{3+} (x=20~80) powders.

Figure S2.

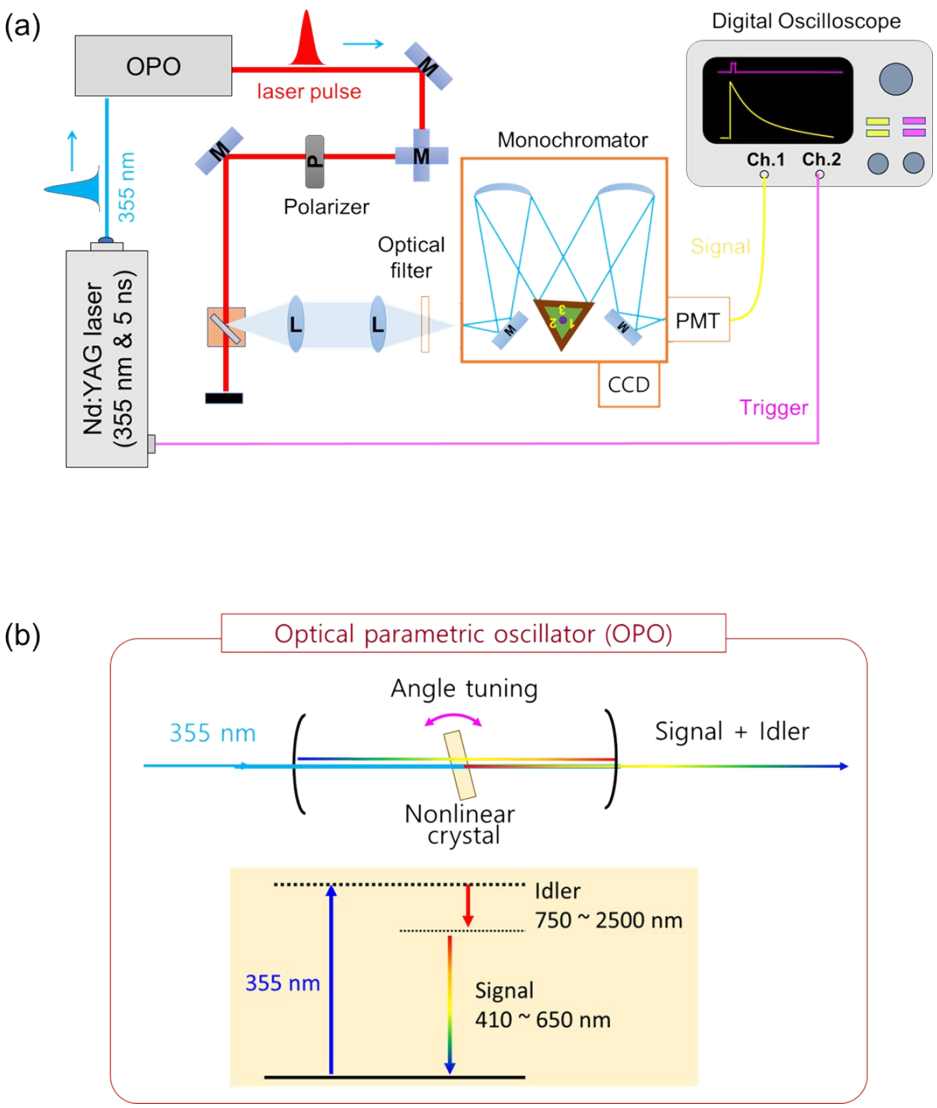

Figure S2. **(a)** Nanosecond time-resolved PL experimental setup. **(b)** Schematic illustration of an optical parametric oscillator (OPO) and nonlinear optical processes.

Figure S3.

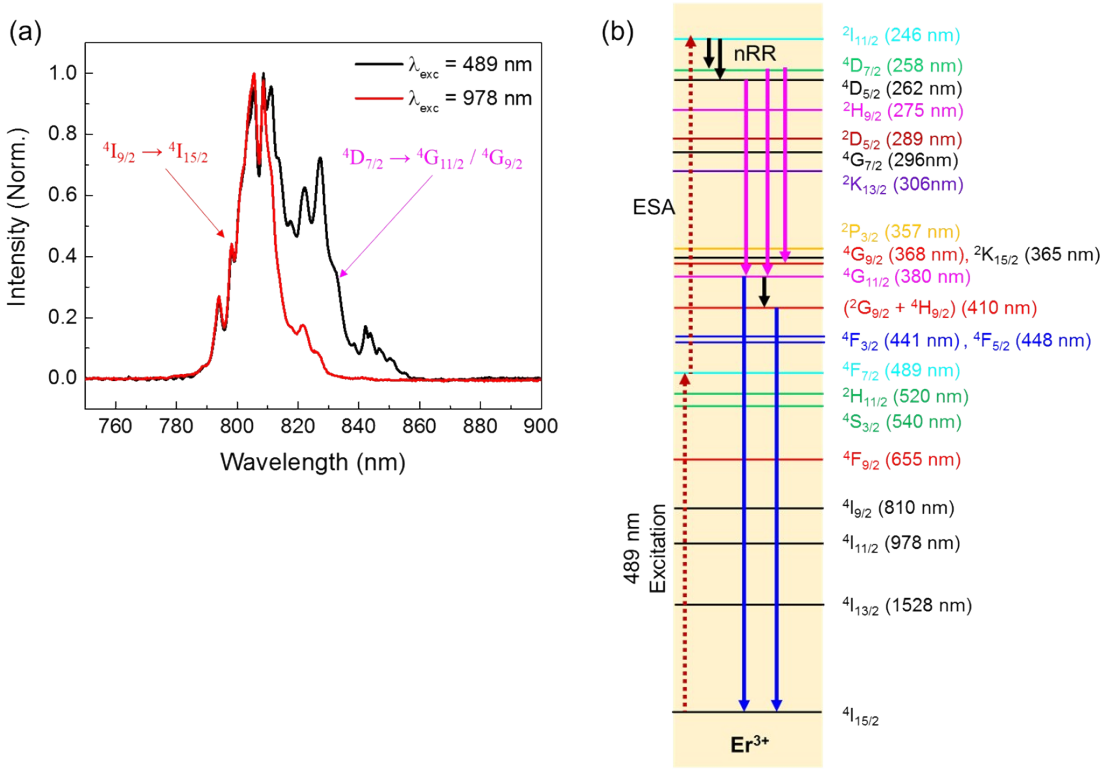

Figure S3. (a) PL spectra measured with $NaErF_4$ powders (λ_{exc}= 489 and 978 nm). The excitation laser power is 20 mW. **(b)** The energy level diagram of Er^{3+}. The margent arrows indicate that the radiative relaxation from higher electronic states ($^2I_{11/2}$, $^2D_{7/2}$ and $^2D_{5/2}$ states) to $^2G_{11/2}$ and $^2G_{9/2}$ states. The non-radiative relaxations (nRR) are indicated by the black arrows.

Figure S4.

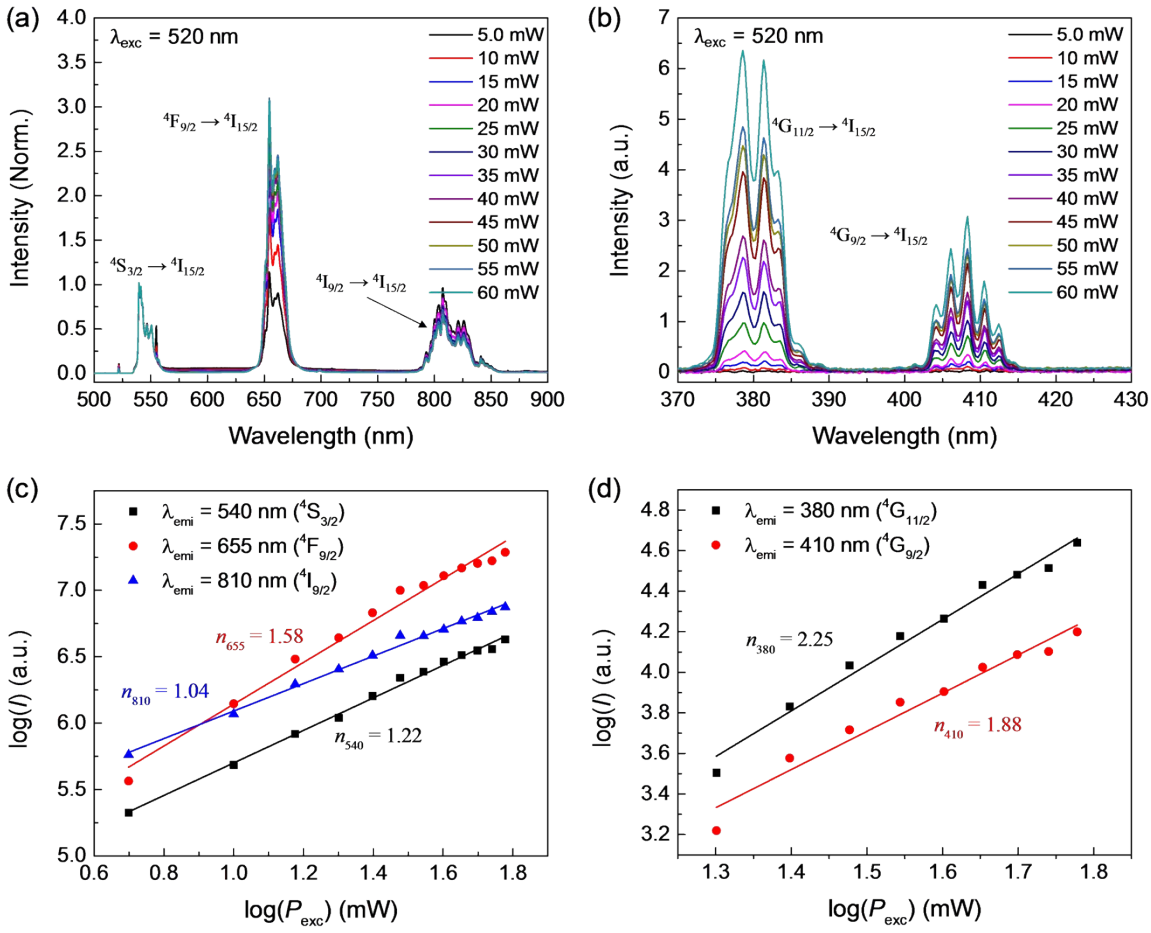

Figure S4. (a) Power-dependent PL spectra measured with $NaErF_4$ powders (λ_{exc}= 520 nm). A 532 nm Raman edge filter was used to block the Rayleigh scattering. The emission at ~520 nm is not shown. All PL spectra were normalized based on the peak at ~540 nm ($^4S_{3/2} \rightarrow {}^4I_{15/2}$) for comparison. **(b)** Power-dependent emission peaks at ~380 and ~410 nm. **(c)** and **(d)** The log-log plot of the emission intensities (I) against excitation laser power (P_{exc}). Data points are experimental results and the line is the fit to Eq. (1). The slopes (n) are given.

Figure S5.

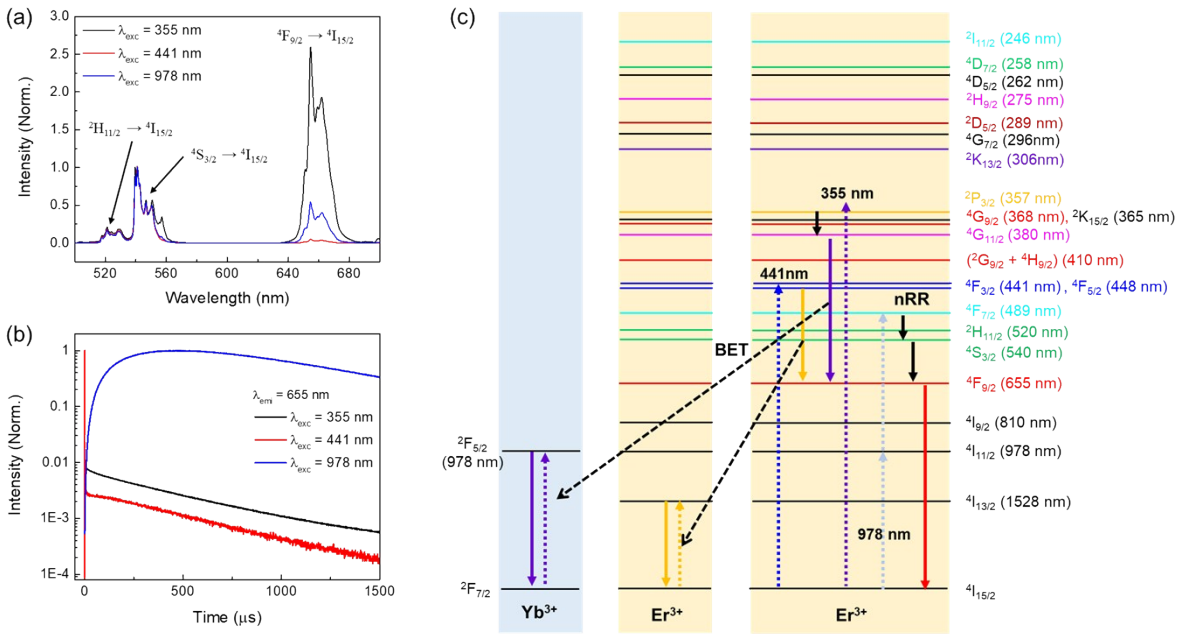

Figure S5. (a) PL spectra and **(b)** time resolved PL signals measured with $NaYF_4:Yb^{3+}:Er^{3+}(Y^{3+}:Yb^{3+}:Er^{3+}=78:20:2)$ powders (λ_{exc}= 355, 441, and 978 nm). PL spectra are normalized based on the peak at ~540 nm. The excitation laser power is set to 20 mW. **(c)** The energy level diagram and the possible transitions. The resonance energy transfers are indicated by the dashed arrows.

Figure S6.

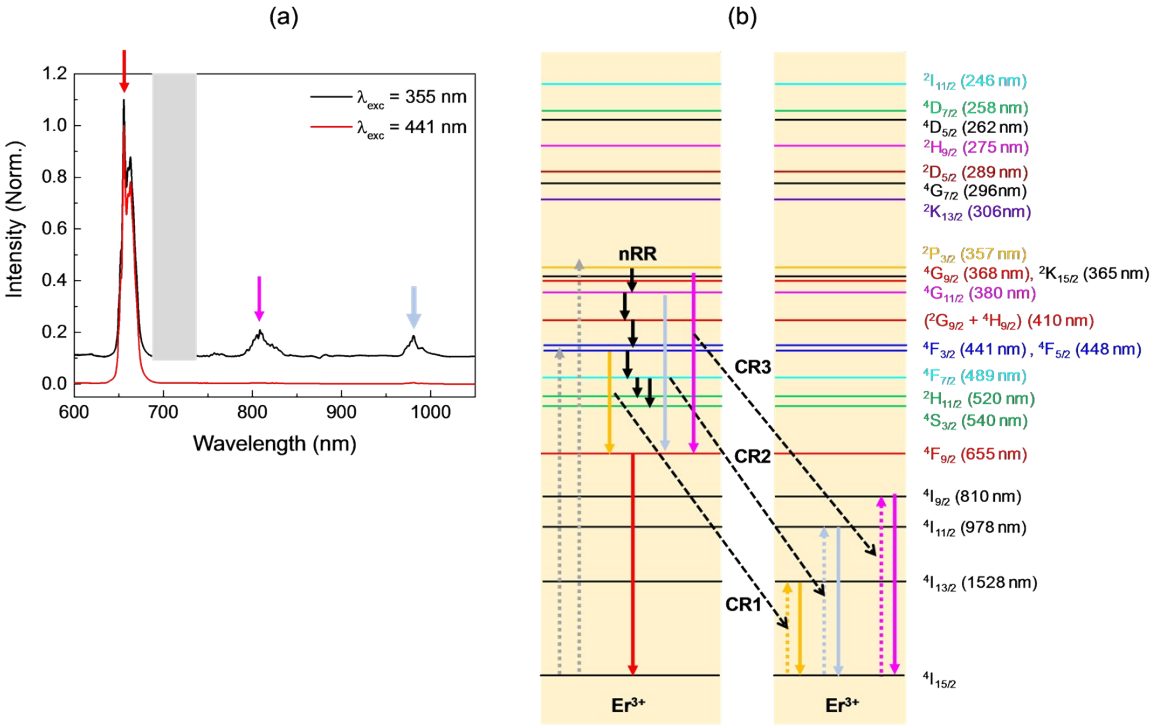

Figure S6. (a) PL spectra measured with $NaErF_4$ powders (λ_{exc}= 355 and 441 nm). PL spectra are normalized based on the peak at 655 nm for comparison. The sub-harmonic of 355 nm was deleted from the PL spectrum. The excitation laser power is set to 20 mW. **(b)** The energy level diagram of Er^{3+}. The peaks at ~810 and 978 nm result from the cross relaxation as indicated by the dashed arrows. The cross relaxation between neighboring Er^{3+} ions are very efficient in $NaErF_4$ powders.

Figure S7.

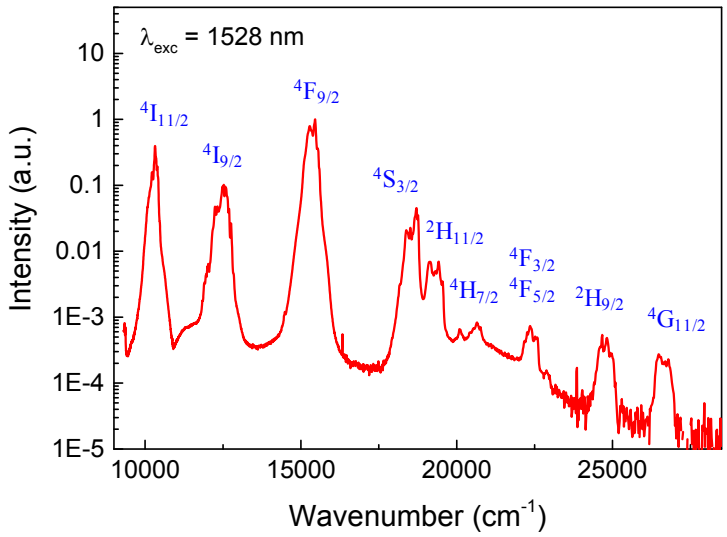

Figure S7. PL spectrum measured with $NaErF_4$ powder (λ_{exc}= 1528 nm). The electronic states are assigned to all the peaks.

Table S1. Particle sizes of Er^{3+}-based upconversion materials

UC material	Particle size (nm)[a]
$NaErF_4$	44.8
$NaYF_4:Er^{3+}$ (80%)	40.1
$NaYF_4:Er^{3+}$ (60%)	34.8
$NaYF_4:Er^{3+}$ (40%)	34.7
$NaYF_4:Er^{3+}$ (20%)	32.1
$NaYF_4:Yb^{3+}$, Er^{3+} (78% : 20% : 2%)	37.6

[a] Particle sizes were estimated from the XRD data and the Scherrer equation.